

On the measurement of directional wave spectra

I. R. Young

Department of Civil & Maritime Engineering, University College, University of New South Wales, Canberra, A.C.T. 2600, Australia

(Received 4 March 1994; revised version received and accepted 28 March 1994)

The directional resolving power of various directional instruments is examined. It is concluded that pitch/roll buoys have intrinsically poor directional resolving power. This finding accounts for the broader directional spreading functions which have been reported for pitch/roll buoy data as compared to spatial array data. Improved instrument performance can be achieved by increasing the number of measurement elements in the measurement system. This is most easily achieved with a spatial array of wave gauges. A rational method for the design of spatial arrays is presented. This technique allows the number and placement of gauges in an array to be determined so as to achieve the desired instrument performance.

1 INTRODUCTION

For a variety of applications, including coastal and ocean engineering, ship routing and the interpretation of remotely sensed data, information on the directional wave spectrum is desirable. Knowledge of the integrated or one-dimensional spectrum is considerable, due largely to field measurements such as the Joint North Sea Wave Project (JONSWAP).¹ A similar situation, however, does not exist in the case of directional spectra. This is largely due to the added complexity and cost of directional measurements as well as the increased sophistication required in data analysis. As will be shown, both the instrumentation chosen and the analysis technique adopted can have significant effects on the resulting directional spectrum.

There are two common in-situ techniques for the measurement of directional wave spectra: pitch/roll buoys (or pressure/velocity (p, u, v) meters) and spatial arrays of wave gauges. The directional wave spectrum is typically discretized into frequency and direction bins. An adequate description of this two-dimensional form may require as many as 30 directional components at each frequency. Since measurement instruments provide only a small number of quantities from which these components are to be determined (three in the case of a buoy, the number of sensors in the case of a spatial array), the problem is under-determined and the various analysis techniques provide only an estimate of the true directional spectrum. As a result, both the number of quantities the instrument measures and the analysis technique may have significant effects on the result. Remote techniques, such as HF Radar (Barrick,²)

Synthetic Aperture Radar (Hasselmann *et al.*,³) Surface Contour Radar (Walsh *et al.*,⁴) Stereo Photography (Holthuijsen⁵) and others can also be used to determine directional spectra. These techniques will not be considered in this paper.

Proposed analytical forms for the directional spreading function yield quite different results as to the spectral spreading for fetch limited conditions. This paper shows that this divergence is consistent with the measurement instrument and analysis technique used. The arrangement of the paper is as follows. In Section 2, proposed forms for the directional spreading function are presented and their considerable differences highlighted. Section 3 presents the commonly used techniques for the analysis of both buoy and array data. An intercomparison of these techniques is presented in Section 4, thus explaining the differences in reported spreading functions. A rational basis for the design of measurement arrays is then presented in Section 5, followed by conclusions in Section 6.

2 PROPOSED DIRECTIONAL SPREADING FUNCTIONS

It is common practice to consider the directional frequency spectrum, $F(\omega, \theta)$, where ω is the radian measure of frequency and θ the wave propagation direction, in terms of the one-dimensional spectrum, $E(\omega)$, as,⁶

$$F(\omega, \theta) = E(\omega) D(\omega, \theta) \quad (1)$$

The directional spreading function, $D(\omega, \theta)$ must satisfy

the condition

$$\int D(\omega, \theta) d\theta = 1 \quad (2)$$

Based on field data, analytical forms for $D(\omega, \theta)$ have been proposed by Mitsuyasu *et al.*,⁷ Hasselmann *et al.*⁸ and Donelan *et al.*⁹ Mitsuyasu *et al.*⁷ considered data collected with a cloverleaf buoy which measures six quantities related to the surface wave field (the vertical acceleration of the water surface, η_{tt} , the wave slope, η_x , η_y and the surface curvature, η_{xx} , η_{yy} , η_{xy}). Their analysis procedure considered only the surface acceleration and slope information, reducing the data to that which would be collected with a pitch/roll buoy. Following Longuet-Higgins *et al.*⁶ they represented $D(\omega, \theta)$ in the form

$$D(\omega, \theta) = Q(s) \cos^{2s} \frac{(\theta - \theta_m(\omega))}{2} \quad (3)$$

where $Q(s)$ is a normalization factor required to satisfy eqn (2) and θ_m is the mean wave direction at frequency ω . Based on their data, Mitsuyasu *et al.*⁷ parameterized s as

$$s = \begin{cases} s_p \left(\frac{\omega}{\omega_p}\right)^5 & \omega < \omega_p \\ s_p \left(\frac{\omega}{\omega_p}\right)^{-2.5} & \omega \geq \omega_p \end{cases} \quad (4)$$

where s_p is the value of s at the frequency of the spectral peak, ω_p , given by

$$s_p = 11.5 \left(\frac{U_{10}}{C_p}\right)^{-2.5} \quad (5)$$

$C_p = g/\omega_p$ is the deep water phase speed of components at the spectral peak and U_{10} the wind speed at a reference height of 10 m.

Hasselmann *et al.*⁸ considered pitch/roll buoy data, also representing their data in the form of eqn (3) but with a different parameterization for s :

$$s = \begin{cases} 6.97 \left(\frac{\omega}{\omega_p}\right)^{4.06} & \omega < 1.05\omega_p \\ 9.77 \left(\frac{\omega}{\omega_p}\right)^\mu & \omega \geq 1.05\omega_p \end{cases} \quad (6)$$

where μ has a weak dependence on wave age:

$$\mu = -2.33 - 1.45 \left(\frac{U_{10}}{C_p} - 1.17\right) \quad (7)$$

Based on data from an array of 14 wave gauges, Donelan *et al.*⁹ found that the form represented by eqn (3) did not adequately represent their data and adopted the alternative form

$$D(\omega, \theta) = 0.5\beta \operatorname{sech}^2 \beta(\theta - \theta_m(\omega)) \quad (8)$$

They found that β varied as a function of

non-dimensional frequency, ω/ω_p . Their data, however, extended only to $\omega/\omega_p = 1.6$ and beyond this point they assumed β was constant. Banner¹⁰ reviewed this conclusion in the context of high frequency stereo photography data and concluded that the assumption that $\beta = \text{constant}$ for $\omega/\omega_p > 1.6$ was unreasonable. He proposed a formulation for β beyond $1.6\omega_p$ which is combined with the Donelan *et al.*⁹ parameterizations for $\omega < 1.6\omega_p$ in eqn (9) below:

$$\beta = \begin{cases} 2.61 \left(\frac{\omega}{\omega_p}\right)^{1.3} & 0.56 < \omega/\omega_p < 0.95 \\ 2.28 \left(\frac{\omega}{\omega_p}\right)^{-1.3} & 0.95 < \omega/\omega_p < 1.6 \\ 10\{-0.4 + 0.8393 \exp[-0.567 \ln((\omega/\omega_p)^2)]\} & \omega/\omega_p > 1.6 \end{cases} \quad (9)$$

2.1 Comparison of spreading functions

Figure 1 shows the directional spreading functions calculated using eqns (4), (6) and (9) at frequencies of $\omega/\omega_p = 1, 2$ and 3 and values of the inverse wave age $U_{10}/C_p = 1, 1.3$ and 2. The differences between these proposed formulations are significant. It is clear that the spreading functions derived from pitch/roll buoy data yield broader spreading functions than the spatial array data.⁹ A clearer representation of the differences is evident if the mean spectral width, $\bar{\theta}$ is examined:

$$\bar{\theta}(\omega) = \frac{\int_0^{2\pi} F(\omega, \theta) \theta d\theta}{\int_0^{2\pi} F(\omega, \theta) d\theta} \quad (10)$$

Figure 2 shows the mean spectral width as a function of ω/ω_p and inverse wave age, U_{10}/C_p for each of the above spreading parameterizations.

All representations indicate that the spreading is narrowest in the region of the spectral peak, becoming broader at frequencies both above and below ω_p . The Donelan *et al.*⁹ formulation is not a function of wave age whereas the representations of both Mitsuyasu *et al.*⁷ and Hasselmann *et al.*⁸ indicate increased broadening as a function of wave age (decreasing U_{10}/C_p). This dependence on wave age is considerably stronger in the Mitsuyasu *et al.*⁷ formulation than that of Hasselmann *et al.*⁸ Whether the directional spreading should be a function of wave age has been discussed by both Hasselmann *et al.*⁸ and Donelan *et al.*⁹ The answer to this question depends on which physical process is controlling the directional spreading. If it is nonlinear interactions within the spectrum, as proposed by Hasselmann,¹¹ then wave age should play no role. If, however, atmospheric input plays a role, the spreading should be dependent on wave age. Young and Van

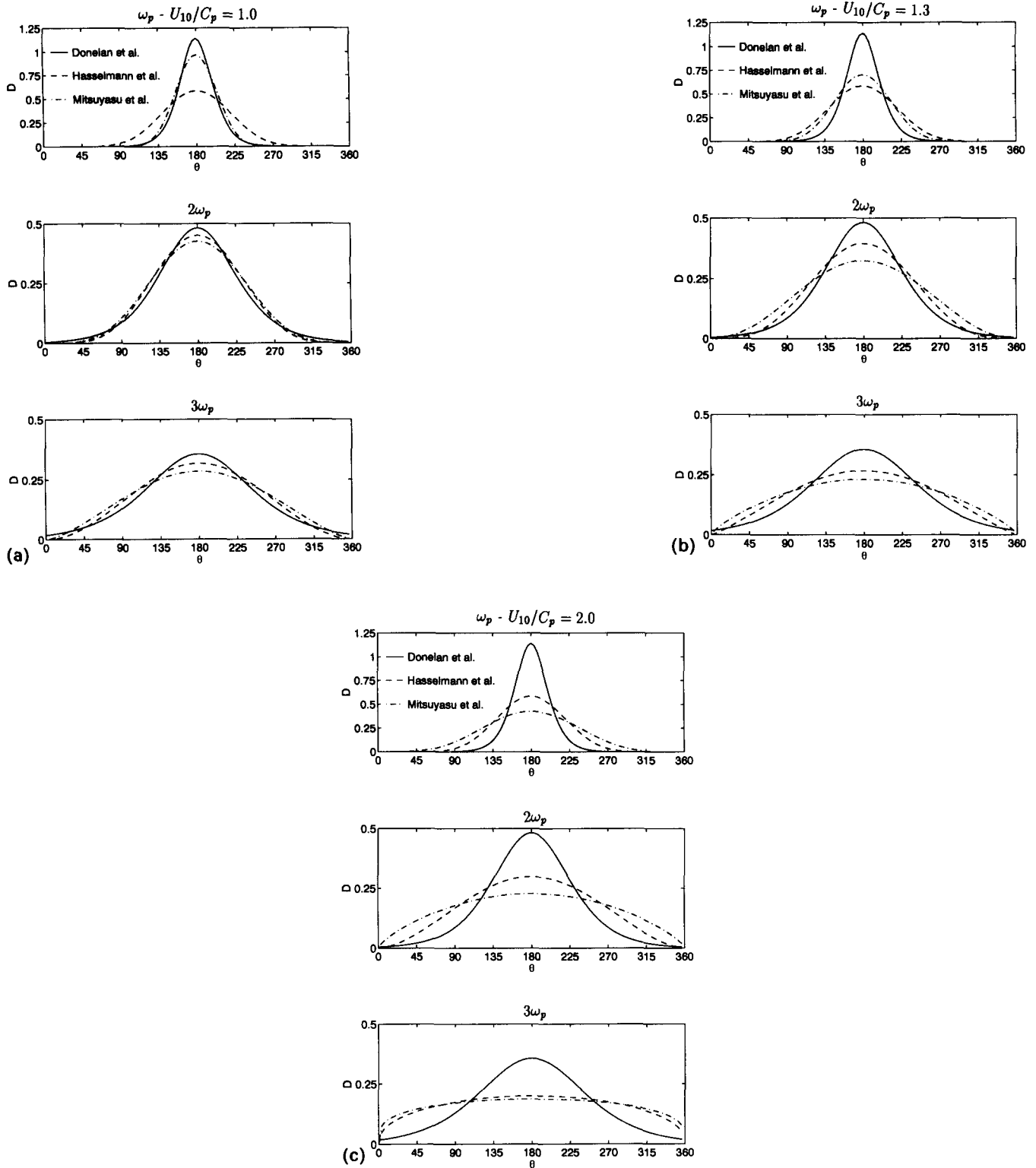


Fig. 1. (a) The directional spreading function D as proposed by Mitsuyasu *et al.*,⁷ Hasselmann *et al.*⁸ and Donelan *et al.*⁹ for $\omega = \omega_p$, $2\omega_p$ and $3\omega_p$ and $U_{10}/C_p = 1.0$. (b) As for Fig. 1(a) but for $U_{10}/C_p = 1.3$. (c) As for Fig. 1(a) but for $U_{10}/C_p = 2.0$.

Vledder¹² and Banner and Young¹³ have investigated the development of the directional spectrum under fetch limited conditions using a spectral model with a full solution to the nonlinear source term. They find that the directional spreading is almost completely controlled by

nonlinear interactions, input playing only a very minor role. Hence, it would appear that either no dependence on wave age (Donelan *et al.*⁹) or a weak dependence (Hasselmann *et al.*⁸) is most appropriate.

In interpreting these proposed spreading functions,

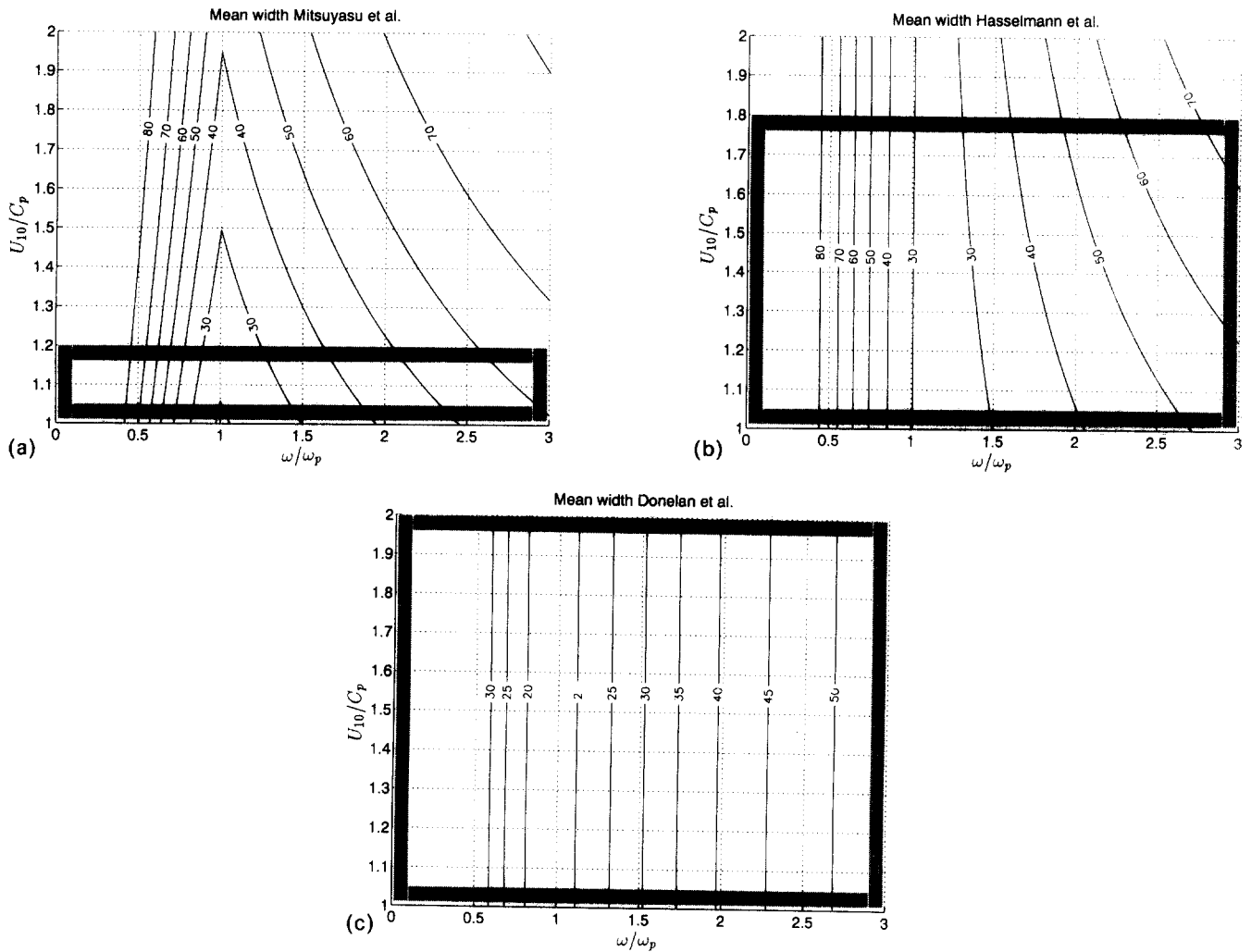


Fig. 2. The mean directional width $\bar{\theta}$ as a function of inverse wave age and frequency as proposed by: (a) Mitsuyasu *et al.*,⁷ (b) Hasselmann *et al.*,⁸ and (c) Donelan *et al.*⁹ The parameter range for which data was collected is outlined by the shading.

the parameter range of the data upon which the various formulations are based should be noted. Table 1 shows the appropriate regions of data validity for each of these studies.

These regions of data validity have been marked on Fig. 2. It is clear that the data upon which the formulation of Mitsuyasu *et al.*⁷ are based, cover a very small range of wind-sea wave ages and hence the accuracy of the strong dependence on wave age in this formulation must be questioned. Over the parameter range for which the data of Mitsuyasu *et al.*⁷ and Hasselmann *et al.*⁸ overlap, there is in fact quite good agreement between these formulations (see Fig. 1(a) and

(b)). These formulations are however considerably broader than those of Donelan *et al.*⁹

3 ANALYSIS TECHNIQUES FOR DIRECTIONAL DATA

Donelan *et al.*⁹ have indicated that the differences in directional spreading described in Section 2 are caused by a combination of the directional resolving power of the instruments and the adopted analysis technique. In this section the various analysis techniques will be cast in a common mathematical framework for subsequent comparison in Section 4.

The time and space variant water surface elevation, $\eta(\mathbf{x}, t)$ is commonly represented as

$$\eta(\mathbf{x}, t) = \iint e^{i(\mathbf{k} \cdot \mathbf{x} - \omega t)} Z(\mathbf{k}, \omega) d\mathbf{k} d\omega \quad (11)$$

where $Z(\mathbf{k}, \omega)$ is the complex Fourier amplitude of the component with wavenumber, \mathbf{k} and frequency, ω .

Table 1. Parameter range for the data from published directional formulations

Study authors	ω/ω_p	U_{10}/C_p
Donelan <i>et al.</i> /Banner	< 5	1-6
Mitsuyasu <i>et al.</i>	< 3	0.6-1.2
Hasselmann <i>et al.</i>	< 3	1-1.8

The wavenumber–frequency spectrum can be represented in terms of the Fourier coefficients by

$$S(\mathbf{k}, \omega) d\mathbf{k} d\omega = \langle Z(\mathbf{k}, \omega) Z^*(\mathbf{k}, \omega) \rangle \quad (12)$$

where the angle brackets denote an ensemble average and the star notation the complex conjugate. Generally, the water surface elevation η is not measured directly, but some quantity ξ which can be related to η (e.g. pressure, p or slope, η_x). Following Isobe *et al.*,¹⁴ the general quantity, ξ can be related to η through the definition of a transfer function, H :

$$H(\mathbf{k}, \omega) = (\cos \theta)^\alpha (\sin \theta)^\beta G(k, \omega) \quad (13)$$

The quantities α , β and G depend on the quantity being measured, ξ , and are tabulated in Appendix 1.

Substitution of eqn (13) into eqn (11) yields

$$\xi(\mathbf{x}, t) = \iint H(\mathbf{k}, \omega) e^{i(\mathbf{k} \cdot \mathbf{x} - \omega t)} Z(\mathbf{k}, \omega) d\mathbf{k} d\omega \quad (14)$$

The cross-spectrum, $\Phi_{mn}(\omega)$ between any two of the quantities measured, $\xi_m(\mathbf{x}_m, t)$ and $\xi_n(\mathbf{x}_n, t)$ is

$$\begin{aligned} \Phi_{mn}(\omega) d\omega = & \left\langle \int H_m(\mathbf{k}, \omega) e^{i(\mathbf{k} \cdot \mathbf{x}_m)} Z(\mathbf{k}, \omega) d\mathbf{k} \right. \\ & \left. \times \int H_n^*(\mathbf{k}', \omega) e^{-i(\mathbf{k}' \cdot \mathbf{x}_n)} Z^*(\mathbf{k}', \omega) d\mathbf{k}' \right\rangle \end{aligned} \quad (15)$$

Since Z is a random variable $\langle Z(\mathbf{k}, \omega) Z^*(\mathbf{k}', \omega) \rangle = 0$ for $\mathbf{k} \neq \mathbf{k}'$ and eqn (15) becomes

$$\Phi_{mn}(\omega) = \int H_m(\omega) H_n^*(\omega) e^{-i\mathbf{k} \cdot (\mathbf{x}_n - \mathbf{x}_m)} F(\omega, \theta) d\theta \quad (16)$$

where the dispersion relationship has been used to introduce the directional frequency spectrum $F(\omega, \theta)$ in place of the wavenumber–frequency spectrum, $S(\mathbf{k}, \omega)$.

The determination of the directional spectrum, $F(\omega, \theta)$ can then be achieved by the inversion of eqn (16). In practice, however, this is not straightforward. At any given frequency, ω , it is desired to define $F(\omega, \theta)$ at sufficient discrete values of θ to accurately define the directional spreading. The number of measured cross-spectra which can be used to determine these discrete values of the spectrum are limited by the number of independent quantities measured by the instrument. For common instruments the number of cross-spectra are far less than the desired number of discrete values of the directional spectrum. The problem is under-defined. A number of possible solutions to this problem have been proposed,^{6,14–19} the two most commonly used being described in detail below.

3.1 Solution by Fourier Expansion (FEM)

Longuet-Higgins *et al.*⁶ expanded the directional spreading function, $D(\omega, \theta)$ as a Fourier series of the

form

$$D(\omega, \theta) = a_0 + \sum_{p=1}^M a_p(\omega) \cos p\theta + b_p(\omega) \sin p\theta \quad (17)$$

If there are N quantities being measured by the instrument, Φ_{mn} is an $N \times N$ matrix, but since $\Phi_{mn} = \Phi_{nm}^*$ there are effectively only $N(N+1)/2$ unique cross-spectra. Equation (17) has a total of $2M+1$ unknowns (the coefficients a_p, b_p). Therefore, provided $M \leq N(N+1)/4 - 1/2$ the system of equations can be directly solved for the coefficients, thus defining the directional spreading function through eqn (17). As the number of measured quantities, N , is decreased, the Fourier series (eqn (17)) must be progressively truncated at lower order, M . For instance, in the case of a pitch/roll buoy, $N = 3$ and hence M must be truncated at 2. A consequence of this truncation is that negative lobes develop in the resulting directional spreading function.⁶ In order to overcome this problem, Longuet-Higgins *et al.* proposed that D be constrained to the analytical form represented by eqn (3). The two parameters in this functional form θ_m and s can be determined from the coefficients of eqn (17):

$$\theta_m = \tan^{-1} \left(\frac{b_1}{a_1} \right) \quad (18a)$$

$$s = \frac{r_1 \pi}{1 - r_1 \pi}; \quad r_1^2 = a_1^2 + b_1^2 \quad (18b)$$

This is the analysis technique used by both Mitsuyasu *et al.*⁷ and Hasselmann *et al.*⁸ For brevity, the term Fourier Expansion Method or FEM is used in the remainder of this paper to describe this technique.

3.2 Solution by Maximum Likelihood Method (MLM)

Solution by the FEM as represented by eqn (18) constrains the directional spreading function to a predetermined model form. A number of model independent formulations have also been proposed. The most commonly used of these is the Maximum Likelihood Method (MLM).^{14,15}

As its name suggests, the MLM attempts to determine the directional spectrum which has the maximum likelihood of conforming to the limited number of cross-spectral estimates. As developed by Isobe *et al.*,¹⁴ the energy incident from angle θ is evaluated by minimizing the influence from all other components. This minimization is achieved through the use of the Lagrange multiplier theory. The final result is

$$F(\omega, \theta) = \frac{Q(\omega)}{\sum_m \sum_n \Phi_{mn}^{-1}(\omega) H_m^*(\omega) H_n(\omega) e^{i\mathbf{k} \cdot (\mathbf{x}_n - \mathbf{x}_m)}} \quad (19)$$

where $Q(\omega)$ is a normalization factor such that the total energies of the directional and one-dimensional spectra

are equivalent (eqn (3)). Details of the application of the MLM to both pitch/roll buoy systems and spatial arrays are given in Appendix 2.

3.3 Other solution techniques

In addition to the FEM and the MLM there are a number of alternative techniques which have been used for the extraction of directional spectra from measured data. These techniques include: the Iterative Maximum Likelihood Method (Pawka²⁰), the Normalized Maximum Likelihood Method (Brissette and Tsanis¹⁸) and the Maximum Entropy Method (Lygre and Krogstad²¹). A comparison of the advantages and disadvantages of these techniques has been reported by Tsanis and Brissette.¹⁹ Based on their results, it appears that the MLM produces reasonable results under a wide range of conditions. Although the Normalized Maximum Likelihood Method can produce superior results, the rather subjective choices which must be made in the normalization make it unattractive for the present application. As a result only the FEM (due to its wide usage) and the MLM are considered in the remainder of this paper.

4 THE CONSEQUENCES OF ANALYSIS TECHNIQUE AND INSTRUMENT TYPE

Donelan *et al.*⁹ have indicated that pitch/roll buoys have intrinsically poor directional resolving power and Isobe *et al.*¹⁴ have indicated that the MLM is the analysis technique with the highest directional resolving capabilities. These statements tend to suggest that both the selection of the instrument and the analysis technique will influence the results. In this section a number of numerical experiments are conducted to determine the sensitivity of the derived spectra to these quantities.

4.1 A comparison between FEM and MLM

In order to compare these two analysis techniques an input directional spectrum with a spreading function of the form proposed by Donelan *et al.*⁹ (eqn (8)) was defined. To make the test as demanding as possible, the relatively large value of $\beta = 3$ was selected (narrow directional spreading). A small amount (1% of maximum spectral ordinate) of incoherent noise was also added to the spectrum. With the spectral form defined, the cross-spectral matrix can be determined from eqn (16). These cross-spectra can then be run through the analysis techniques and the resulting directional spreading compared with the input form.

Figure 3 shows comparisons between the input and calculated directional spreading functions for a pitch/roll buoy system derived with both the FEM and MLM. Both analysis techniques produce directional spreading which is too broad and significantly underestimate the

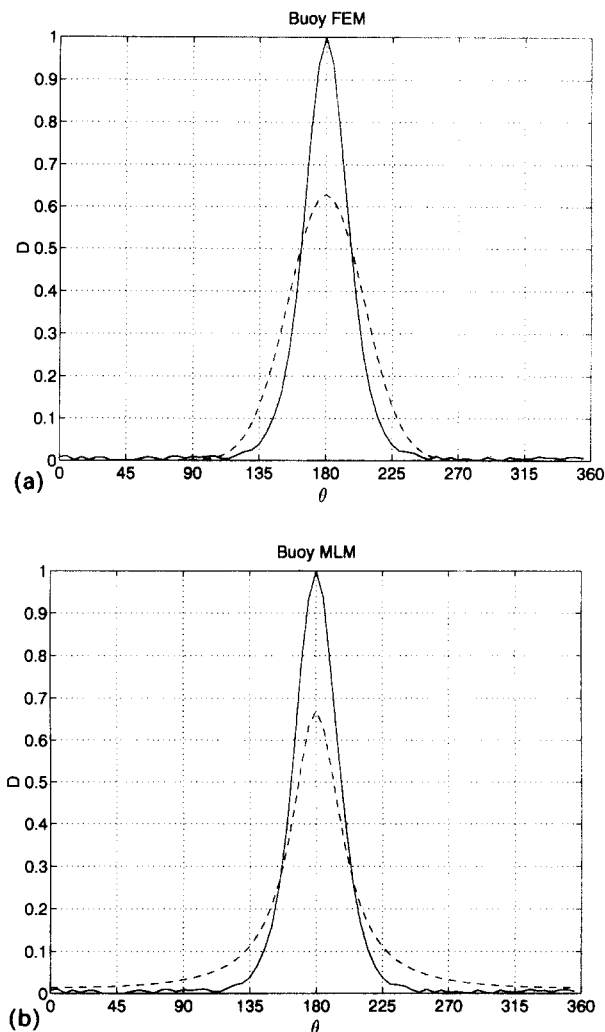


Fig. 3. (a) A comparison between an input directional spreading function of the form (8) with $\beta = 3$ (solid line) and the derived spreading function (dashed line) for a pitch/roll buoy analysed using the FEM. (b) As for Fig. 3(a) but analysed using the MLM.

magnitude of the narrow directional distribution. As expected, the MLM is marginally superior but the differences are only minor. It is interesting to note that if the small amount of noise is removed from the input spectrum, the resulting fit is much improved. It is felt, however, that the addition of the noise more closely simulates the situation encountered in reality.

Since the MLM is not constrained by the adoption of a specific directional representation, in theory, it has the ability to reproduce skewed or bimodal directional forms. Fourier expansion can, however, produce only one symmetric peak at any frequency. This is demonstrated in Fig. 4, where a second peak, half the magnitude of the original peak and separated by 45° , has been added to the input form. The FEM attempts to approximate this bimodal distribution with a single peak centred about the weighted mean direction. Although the MLM cannot accurately separate these two narrow

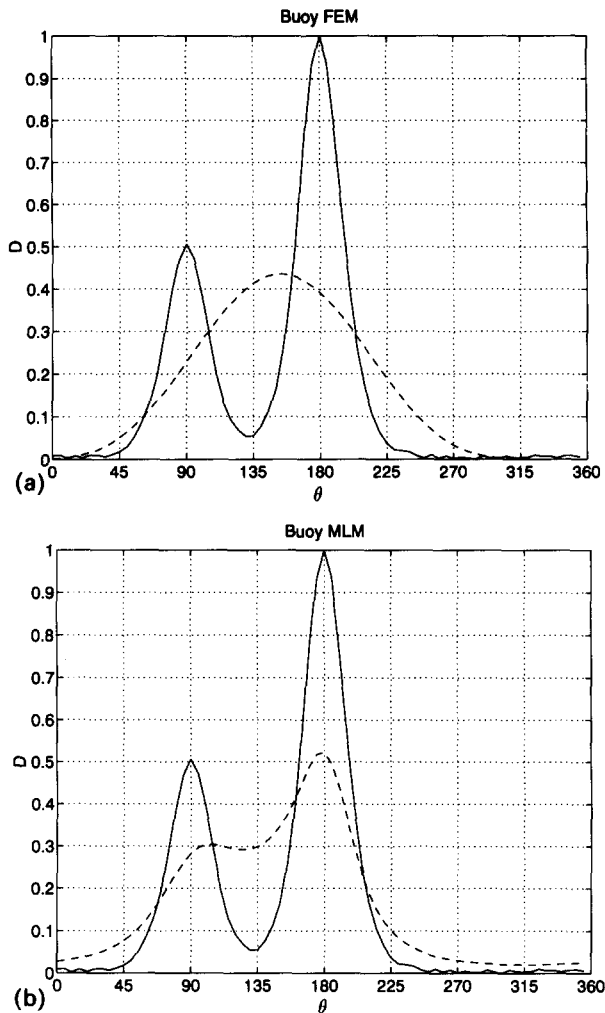


Fig. 4. (a) Input (solid line) and derived (dashed line) bimodal spreading functions for a pitch/roll buoy analysed using the FEM. (b) As for Fig. 4(a) but analysed using the MLM.

and closely spaced peaks, it clearly produces a superior result to the FEM with the existence of both peaks being clear.

Figures 3 and 4 generally produce disappointing results, the conclusion being that neither analysis method is capable of producing adequate results with the limited amount of data available from a pitch/roll buoy. The analysis and hence the conclusions are the same for any instrument with three elements. Examples of this include: p,u,v meters and three element gauge arrays.

4.2 Influence of the number of measurement elements

The obvious conclusion from Section 4.1 is that the number of measurement elements should be increased. This is really not practical in a floating buoy system, although clover-leaf buoys do increase the effective number of measurement elements from three to six. Spatial arrays can, however, have any number of

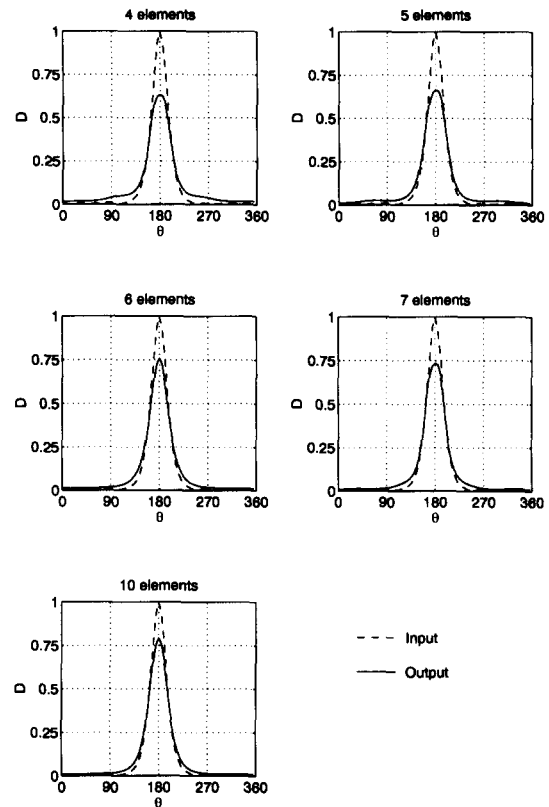


Fig. 5. Input (dashed line) and derived (solid line) spreading functions for centred regular spatial arrays with different numbers of measurement elements.

elements, although they quickly become cumbersome. Figure 5 shows the results for the same input spectrum as used in Fig. 3 for spatial arrays with 4, 5, 6, 7 and 10 elements respectively. In all cases the arrays were symmetric with one gauge at the centre and the remaining gauges evenly distributed at the same radius around this central gauge. The MLM was used for the analysis. Not surprisingly, increasing the number of gauges progressively improves the results. As the number of gauges increases, the peak of the output spreading function increases and the overestimation in energy at angles away from the dominant wave direction decreases.

5 OPTIMUM DESIGN OF SPATIAL ARRAYS

The performance of a spatial array is not solely determined by the number of array elements. This is clearly illustrated in Fig. 5. Comparison of the results for the 6 and 7 element arrays shows that although the 7 element array generally produces a better approximation to the directional distribution, in the mean direction the 6 element array is slightly superior. The actual geometry of the gauges in the array and their spacing

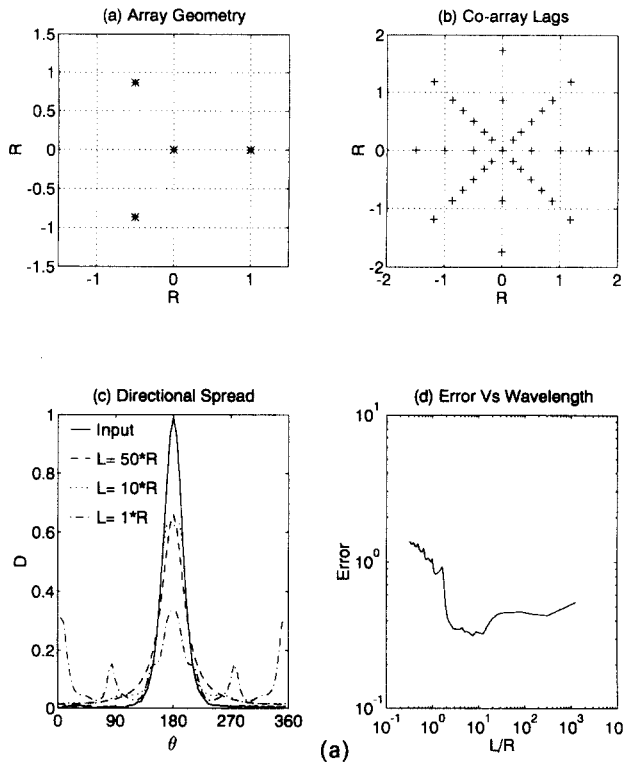


Fig. 6(a). Analysis of the performance of a four element array. The individual panels show: (a) the array configuration; (b) the co-array lags; (c) the input (solid line) and derived (dashed line) directional spreading for waves with wavelengths of R , $10R$ and $50R$; and (d) the mean error function, ϵ .

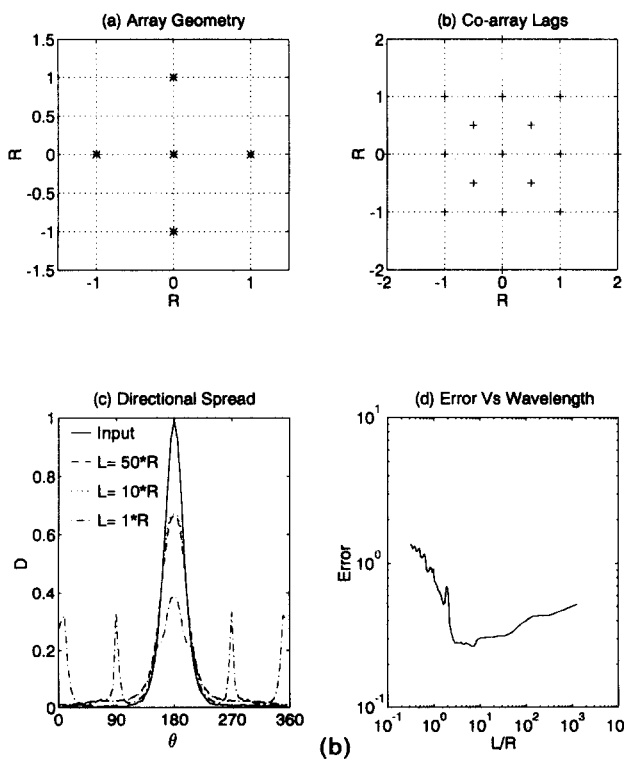


Fig. 6(b). As for Fig. 6(a) but for a five element array.

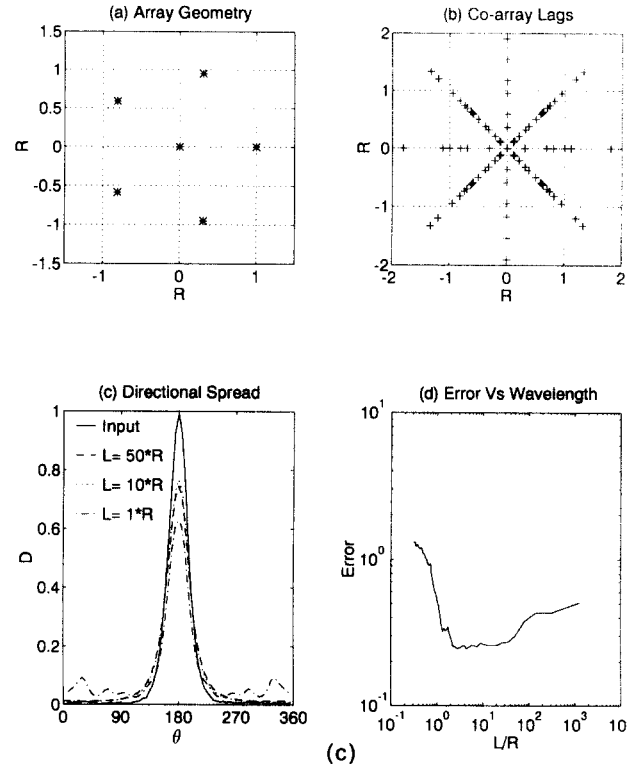


Fig. 6(c). As for Fig. 6(a) but for a six element array.

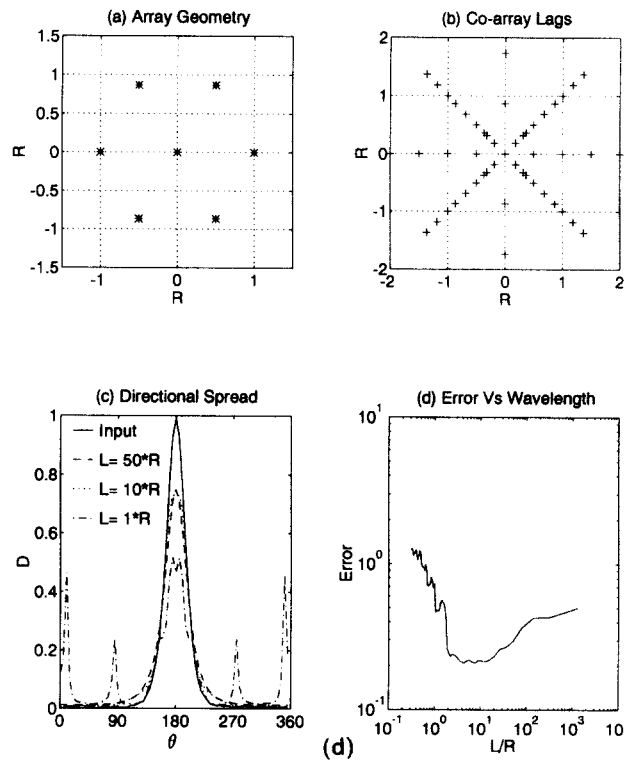


Fig. 6(d). As for Fig. 6(a) but for a seven element array.

relative to the wavelength of the waves being measured are important design considerations. These aspects have been previously noted by Davis and Regier.¹⁶ They point out that the critical parameter in the design of a spatial array is the so called co-array. Here, the co-array

is defined as

$$\zeta_{mn} = \mathbf{k} \cdot (\mathbf{x}_n - \mathbf{x}_m) / k \quad (20)$$

Equation (20) defines the spatial lags between gauges for a given wave direction. Through eqn (16), this quantity influences the cross-spectra from which the directional spectrum is obtained.

An optimum array should have a co-array with lags evenly and densely distributed in both space and direction so as to adequately resolve the anticipated wave system. In order to investigate array geometry and gauge spacing, the 4, 5, 6 and 7 element arrays discussed in Fig. 5 were subjected to further analysis. The results of these analyses are shown in Fig. 6. Rather than consider the results at only a single frequency (or wavelength), the input spectrum was assumed to have the same directional spreading as reported previously but over a wide range of wavelengths. The panels of Fig. 6 show the array geometry, the co-array for waves approaching from eight different directions (every 45°), the input spectrum, $F(\omega, \theta)$ and the array-derived spectrum $\hat{F}(\omega, \theta)$ at wavelengths of 50, 10 and one times the array element spacing R . In addition, the error function, $\epsilon(\omega)$ is also shown, where

$$\epsilon(\omega) = \frac{\int |F(\omega, \theta) - \hat{F}(\omega, \theta)| d\theta}{\int F(\omega, \theta) d\theta} \quad (21)$$

It is clear from the error functions in Fig. 6 that the performance of the arrays is a function of the wavelength-to-gauge spacing ratio, L/R . Not surprisingly, as L/R approaches one, spatial aliasing becomes a problem and the directional spreading is poorly resolved. This is clear both in the plots of the directional spread and in the error functions. At very large values of L/R the cross-spectra are almost all identical and the directional resolution is influenced by the accuracy to which the now poorly conditioned cross-spectral matrix can be inverted. In a practical situation, the measurement accuracy of the gauges will cause a much more rapid degradation of performance than is shown here as L/R becomes large. Between these two limits, the error functions for all the arrays show a relatively wide region where array performance is optimal. The magnitude of the error function progressively decreases as the number of measurement elements increases, indicating improved performance.

Although the number and distribution of lags in the co-array generally increases with the number of elements, for waves travelling along a line of symmetry of the array, many of the lags will be redundant. This is clearly the case for the arrays with 6 and 7 elements. Although the 7 element array has more elements, it has a poorer distribution of lags for waves travelling at 0° and 180° than the 6 element array. This is due to the more complete symmetry of the 7 element or centred hexagon

array as compared to the 6 element or centred pentagon array. Hence, it could be expected that the smaller array would actually have better resolving power in these directions. This explains why the 6 element array produced a slightly larger spectral value in the mean wave direction as shown in Fig. 5. When the error in all directions is considered, however, as reported by $\epsilon(\omega)$, the larger array is still superior.

The arrays considered above are all regular in that the elements are evenly spaced in direction and at a constant radius. The number and distribution of lags in the co-array could be increased by the use of an irregular array. The performance of such an array is shown in Fig. 7. Here a 7 element array is again used. Rather than have the elements arranged as a centred hexagon with radius R , however, this array is in the form of a Mercedes star. Three elements are at a radius R and three at radius $R/2$. As expected, the number and distribution of lags in the co-array has been improved in comparison to the regular 7 element array. The performance of the array has also clearly improved. Although the minimum values of $\epsilon(\omega)$ are the same for the two arrays, the span of values of L/R for which the array performs well is significantly wider for the irregular array. In addition, due to the inclusion of more closely spaced gauges, the minimum value of L/R at which data can be obtained without spatial aliasing has been improved. Hence, this array geometry would be capable of providing directional measurements over a much wider range of spectral frequencies than the regular array.

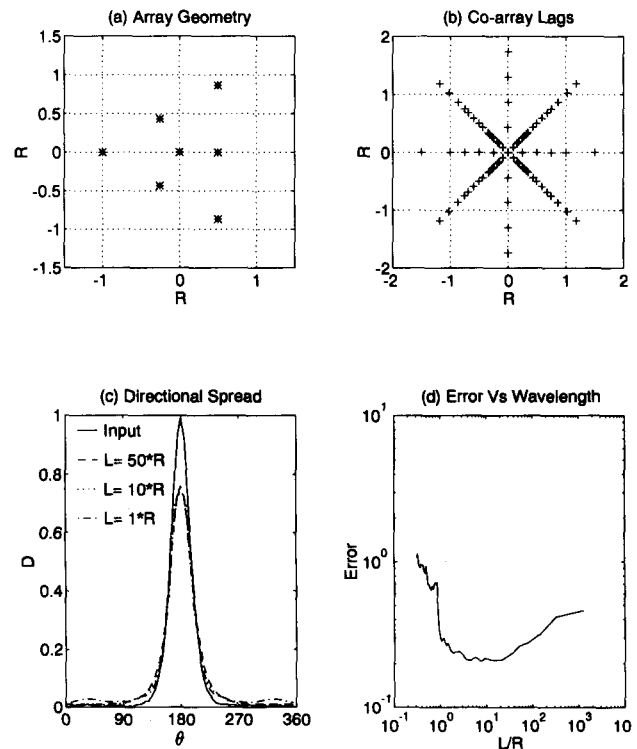


Fig. 7. As for Fig. 6(d) but for a seven element irregularly spaced array.

6 CONCLUSIONS

A review of proposed directional spreading formulations has been conducted. Of the three commonly used formulations, those derived from pitch/roll buoy data (Mitsuyasu *et al.*,⁷ Hasselmann *et al.*⁸) produce significantly broader directional spreading than the spatial array data of Donelan *et al.*⁹ An analysis of the directional resolving power of pitch/roll buoy systems shows that this is a result of the limited number of quantities measured by the instrument. Hence, it can be concluded that, although such instruments can provide an accurate measurement of the mean wave direction, directional spectra will be excessively broad.

A general mathematical framework for the analysis of data from any measurement system is developed and specifically applied to the Fourier Expansion Method (FEM) and Maximum Likelihood Method (MLM). Although the MLM produces a superior representation of the directional spreading when applied to pitch/roll buoy data, the improvement is only marginal.

An improvement in the directional resolving power of a sensor can only be achieved by increasing the number of measurement elements in the sensor. This is clearly demonstrated by investigating the performance of spatial arrays with varying numbers of elements.

The detailed performance of a spatial array is not only dependent on the number of measurement elements but also the geometrical spacing of elements and the nature of the incident wave spectrum. A rational technique for the design of arrays is developed based on the concept of the co-array. This analysis clearly shows that, for optimum performance, an array should have as many nonredundant spatial lags between elements as possible. As a result, even a symmetric array will not have uniform resolving power for waves incident from all directions.

In the above analyses it is assumed that the measurement instrument is capable of measuring accurately the quantities from which the directional spectrum is obtained. For example, in a floating buoy system it is assumed that the motion of the buoy is such that the surface slope and acceleration can be obtained without error. Obviously this is not the case and such errors will further degrade the resolving power of the instrument. Similar errors will occur in spatial arrays due to the accuracy with which the array geometry is known and in estimates of wave induced currents from current meters which perform some spatial averaging (for example, electro-magnetic current meters).

ACKNOWLEDGEMENTS

The original code from which the MLM analyses conducted in this study were developed was provided

by Will Drennan and Mark Donelan of the Canada Center for Inland Waters. Their assistance is gratefully acknowledged.

REFERENCES

- Hasselmann, K. *et al.* Measurements of wind-wave growth and swell decay during the Joint North Sea Wave Project (JONSWAP). *Dtsch. Hydrog. Z., Suppl. A*, **8**(12) (1973).
- Barrick, D. E. First order theory and analysis of MH/HF/VHF scatter from the sea. *IEEE Trans. Antennas Propag.*, **AP-20** (1972) 2–10.
- Hasselmann, K. *et al.* Theory of synthetic aperture radar ocean imaging: A MARSEN view. *J. Geophys. Res.*, **90** (1985) 4659–86.
- Walsh, E. J., Hancock, D. W. & Hines, D. E. Directional wave spectra measured with surface contour radar. *J. Phys. Oceanogr.*, **15** (1985) 566–92.
- Holthuijsen, L. H. Observations of the directional distribution of ocean-wave energy in fetch-limited conditions. *J. Phys. Oceanogr.*, **13** (1983) 191–207.
- Longuet-Higgins, M. S., Cartwright, D. E. and Smith, N. D. Observations of the directional spectrum of sea waves using the motions of a floating buoy. In *Ocean Wave Spectra*, Prentice-Hall, Inc., Englewood Cliffs, pp. 111–36.
- Mitsuyasu, H., Tasai, F., Suhara, T., Mizuno, S., Ohkuso, M., Honda, T. & Rikiishi, K. Observations of the directional spectrum of ocean waves using a cloverleaf buoy. *J. Phys. Oceanogr.*, **5** (1975) 750–60.
- Hasselmann, D. E., Dunkel, M. & Ewing, J. A. Directional wave spectra observed during JONSWAP 1973. *J. Phys. Oceanogr.*, **10**(8) (1980) 1264–80.
- Donelan, M. A., Hamilton, J. & Hui, W. H. Directional spectra of wind-generated waves. *Phil. Trans. R. Soc. Lond.*, **A315** (1985) 509–62.
- Banner, M. L. Equilibrium spectra of wind waves. *J. Phys. Oceanogr.*, **20** (1990) 966–84.
- Hasselmann, K. On the non-linear energy transfer in a gravity-wave spectrum, Part 1. General theory. *J. Fluid Mech.*, **12** (1962) 481–500.
- Young, I. R. & Van Vledder, G. Ph. A review of the central role of nonlinear interactions in wind-wave evolution. *Phil. Trans. Roy. Soc.*, **342** (1993) 505–24.
- Banner, M. L. & Young, I. R. Modelling spectral dissipation in the evolution of wind waves. Part 1. Assessment of existing model performance. *J. Phys. Oceanogr.*, **24** (1994) 1550–1671.
- Isobe, M., Kondo, K. & Horikawa, K. Extension of MLM for estimating directional wave spectrum. *Symposium on Description and Modelling of Directional Seas*, DHI and MMI, Copenhagen, 1984, pp. 1–15.
- Capon, J. High-resolution frequency-wavenumber spectrum analysis. *Proc. IEEE*, **57** (1969) 1408–18.
- Davis, R. E. & Regier, L. A. Methods for estimating directional wave spectra from multi-element arrays. *J. Marine Res.*, **35** (1977) 453–77.
- Jefferys, E. R., Wareham, G. T., Ramsden, N. A. & Platts, M. J. Measuring directional spectra with MLM. In *Directional Wave Spectra Applications*, ed. R. L. Weigel, pp. 203–19.
- Brissette, F. P. & Tsanis, I. K. Maximum likelihood method techniques for directional analysis of heave-pitch-roll data. *3rd Int. Workshop on Wave Hindcasting and Forecasting*, Montreal, 1993, pp. 1–11.
- Tsanis, I. K. & Brissette, F. P. Methods for directional

spectra measurements by small arrays. *3rd Int. Workshop on Wave Hindcasting and Forecasting*, Montreal, 1992, pp. 12–23.

20. Pawka, S. S. Island shadows in wave directional spectra.

J. Geophys. Res., **88** (1983) 2579–91.

21. Lygre, A. & Krogstad, H. E. Maximum entropy estimation of the directional distribution in ocean wave spectra. *J. Phys. Oceanogr.*, **16** (1986) 2052–60.

APPENDIX 1: VALUES OF THE TRANSFER FUNCTION H (eqn (13))

Measured quantity, ξ	Symbol	$H(\mathbf{k}, \omega)$	$G(k, \omega)$	α	β
Water surface elevation	η	1	1	0	0
Pressure	p	$\rho g \frac{\cosh kz}{\cosh kd}$	$\rho g \frac{\cosh kz}{\cosh kd}$	0	0
Vertical velocity	η_t	$-i\omega$	$-i\omega$	0	0
Vertical acceleration	η_{tt}	$-\omega^2$	$-\omega^2$	0	0
Surface slope (x dir.)	η_x	$ik \cos \theta$	ik	1	0
Surface slope (y dir.)	η_y	$ik \sin \theta$	ik	0	1
Surface curvature (x)	η_{xx}	$-k^2 \cos^2 \theta$	$-k^2$	2	0
Surface curvature (y)	η_{yy}	$-k^2 \sin^2 \theta$	$-k^2$	0	2
Surface curvature (xy)	η_{xy}	$-k^2 \cos \theta \sin \theta$	$-k^2$	1	1
Water particle velocity (x dir.)	u	$\omega \cos \theta \frac{\cosh kz}{\sinh kd}$	$\omega \frac{\cosh kz}{\sinh kd}$	1	0
Water particle velocity (y dir.)	v	$\omega \sin \theta \frac{\cosh kz}{\sinh kd}$	$\omega \frac{\cosh kz}{\sinh kd}$	0	1
Water particle velocity (z dir.)	w	$-i\omega \frac{\sinh kz}{\sinh kd}$	$-i\omega \frac{\sinh kz}{\sinh kd}$	0	0
Water particle accel. (x dir.)	u_t	$-i\omega^2 \cos \theta \frac{\cosh kz}{\sinh kd}$	$-i\omega^2 \cos \theta \frac{\cosh kz}{\sinh kd}$	1	0
Water particle accel. (y dir.)	v_t	$-i\omega^2 \sin \theta \frac{\cosh kz}{\sinh kd}$	$-i\omega^2 \sin \theta \frac{\cosh kz}{\sinh kd}$	0	1
Water particle accel. (z dir.)	w_t	$-\omega^2 \frac{\sinh kz}{\sinh kd}$	$-\omega^2 \frac{\sinh kz}{\sinh kd}$	0	0

APPENDIX 2: APPLICATION OF MLM TO SPECIFIC CASES

1. Pitch/roll buoys

For the specific case of a three-component sensor such as a pitch/roll buoy, which measures η_{tt} , η_x and η_y , the cross-spectral matrix, Φ_{mn} becomes

$$\Phi_{mn} = \begin{pmatrix} \phi_{\eta_{tt}\eta_{tt}} & \phi_{\eta_{tt}\eta_x} & \phi_{\eta_{tt}\eta_y} \\ \phi_{\eta_x\eta_{tt}} & \phi_{\eta_x\eta_x} & \phi_{\eta_x\eta_y} \\ \phi_{\eta_y\eta_{tt}} & \phi_{\eta_y\eta_x} & \phi_{\eta_y\eta_y} \end{pmatrix} \quad (A2.1)$$

The elements of this matrix can be normalized by dividing by the appropriate transfer functions, $G(\omega)$ from Appendix 1. The normalized cross-spectral matrix becomes

$$\Phi'_{mn} = \begin{pmatrix} n_{11} & n_{12} & n_{13} \\ n_{12} & n_{22} & n_{23} \\ n_{13} & n_{23} & n_{33} \end{pmatrix} \quad (A2.2)$$

where

$$n_{11} = \frac{\phi_{\eta_{tt}\eta_{tt}}}{\omega^4}; \quad n_{12} = \frac{\phi_{\eta_{tt}\eta_x}}{-ik\omega^2}; \quad n_{13} = \frac{\phi_{\eta_{tt}\eta_y}}{-ik\omega^2}$$

$$n_{22} = \frac{\phi_{\eta_x\eta_x}}{-k^2}; \quad n_{23} = \frac{\phi_{\eta_x\eta_y}}{-k^2}; \quad n_{33} = \frac{\phi_{\eta_y\eta_y}}{-k^2}$$

A similar result can be obtained for a system of a pressure gauge and two orthogonal current meters, only the transfer functions, $G(\omega)$, being different. Noting that

all elements of (A2.2) are real and that $\mathbf{x}_n = \mathbf{x}_m$ in eqn (19), the matrix (A2.2) can be inverted, eqn (19) finally yielding

$$F(\omega, \theta) = Q(\omega)[M_0 M_2(\gamma^2 \cos^2 \hat{\theta} + \sin^2 \hat{\theta}) - M_1^2 \sin^2(\hat{\theta} - \hat{\theta}_m) - 2M_1 M_2(\gamma^2 \cos \hat{\theta} \cos \hat{\theta}_m + \sin \hat{\theta} \sin \hat{\theta}_m) + M_2^2 \gamma^2]^{-1} \quad (A2.3)$$

where

$$M_0 = n_{11} \quad (A2.4)$$

$$M_1 = \sqrt{(n_{12}^2 + n_{13}^2)} \quad (A2.5)$$

$$M_2 = \frac{n_{22} + n_{33}}{2} + \sqrt{\left(\frac{n_{22} - n_{33}}{2}\right)^2 + n_{23}^2} \quad (A2.6)$$

$$\hat{\theta} = \theta - \theta_p \quad (A2.7)$$

$$\hat{\theta}_m = \theta_m - \theta_p \quad (A2.8)$$

$$\theta_m = \tan^{-1}\left(\frac{n_{13}}{n_{12}}\right) \quad (A2.9)$$

$$\theta_p = \frac{1}{2} \tan^{-1}\left(\frac{2n_{23}}{n_{22} - n_{33}}\right) \quad (A2.10)$$

$$\gamma^2 = \frac{(n_{22} + n_{33}) - \sqrt{(n_{22} - n_{33})^2 + 4n_{23}^2}}{(n_{22} + n_{33}) + \sqrt{(n_{22} - n_{33})^2 + 4n_{23}^2}} \quad (A2.11)$$

where $Q(\omega)$ is a normalization factor (see eqns (2), (3)).

2. Spatial array of gauges

For the case of a spatial array of wave gauges, H_m and H_n are both equal to one in eqn (19) yielding

$$F(\omega, \theta) = Q(\omega) \left[\sum_m \sum_n \Phi_{mn}^{-1}(\omega) e^{ik R_n \cos \theta_n} e^{-ik R_m \cos \theta_m} \right]^{-1} \quad (\text{A2.12})$$

where θ_n is the angle between probe element n and the wave component with propagation direction θ and R_n is the distance of probe element n from a fixed origin. As the cross-spectral matrix is available and the array geometry is known, eqn (A2.12) can be evaluated. The practical details of an implementation are described below.

The directional spectrum, $F(\omega, \theta)$ is to be estimated at discrete frequencies, ω and directions θ from the water surface elevation time histories $\eta_l(t)$ of n_p ($l = 1, n_p$) gauges situated at Cartesian coordinates R_{lx} , R_{ly} . Each of the gauges are sampled coincidentally at a rate $\Delta\omega$.

In order to overcome possible calibration errors between gauges, the $\eta_l(t)$ should be scaled to ensure

they have the same standard deviation. The Fourier transform, $Z_l(\omega)$ is then determined for each gauge and the normalized cross-spectral matrix evaluated

$$\Phi'_{mn}(\omega) = \frac{Z_m(\omega) Z_n^*(\omega)}{|Z_m(\omega)| |Z_n(\omega)|} \quad (\text{A2.13})$$

For each gauge and each discrete angle of wave approach, θ , the complex phase lag between gauge l and the origin is

$$X_l(\omega, \theta) = \exp[-ik(R_{lx} \cos \theta + R_{ly} \sin \theta)] \quad (\text{A2.14})$$

Equation (A2.12) can then be evaluated using the matrix relationship

$$F(\omega, \theta) \propto [X_l^T(\omega, \theta) \Phi_{mn}^{-1}(\omega) X_l(\omega, \theta)]^{-1} \quad (\text{A2.15})$$

where X_l^T represents the transpose of the one-dimensional matrix X_l .

The evaluation of eqn (A2.15) can be complicated by the fact that $\Phi'_{mn}(\omega)$ can become singular. This can be easily overcome by multiplying all off-diagonal values by a small quantity ϵ .¹⁵ The constant of proportionality in eqn (A2.15) can then be determined from the requirement $E(\omega) = \int F(\omega, \theta) d\theta$.